So et al. *Zool. Res.* 2025, 46(6): 1289−1303
https://doi.org/10.24272/j.issn.2095-8137.2025.255
https://cstr.cn/32248.14.zr.2025.255

ZR | Zoological Research

Article Open Access

Prenatal exposure to polystyrene nanoparticles induces neuroimmune dysregulation in the adult mouse brain

Yun Hee So[1,2], Hyun Seung Shin[1,2], Dong Hun Lee[1,2], Min Jae Kim[1,2], Jin Yeop Kim[3], BuHyun Youn[4], Eun-Hee Lee[2,5], Eui-Man Jung[1,2,*]

[1] *Department of Molecular Biology*, *College of Natural Sciences*, *Pusan National University*, *Busan* 46241, *Republic of Korea*
[2] *Institute for Future Earth*, *Pusan National University*, *Busan* 46241, *Republic of Korea*
[3] *BIOLINKs Inc.*, *Chuncheon* 24341, *Republic of Korea*
[4] *Department of Biological Sciences*, *Pusan National University*, *Busan* 46241, *Republic of Korea*
[5] *Department of Microbiology*, *College of Natural Sciences*, *Pusan National University*, *Busan* 46241, *Republic of Korea*

ABSTRACT

Microplastics have been detected in the brain, raising concerns regarding their neurological health impacts. However, the specific cellular targets and functional consequences of their accumulation remain understudied. This study explored the primary brain cell types that internalize polystyrene nanoparticles (PSNs) and investigated their immunological responses. Results showed that PSNs preferentially localized to primary microglia and astrocytes. Functional assays revealed divergent effects on lipopolysaccharide (LPS)-stimulated immune responses in the two cell types: PSNs potentiated LPS-induced activation of microglia, whereas they suppressed activation in astrocytes. Apoptotic responses were likewise cell-type specific, with PSN reducing apoptosis in microglia independently of LPS, but enhancing it in astrocytes. *In vivo*, adult mice exposed to both PSNs and LPS exhibited increased microglial numbers in the hippocampus compared to those receiving LPS alone. These findings demonstrate that PSNs disrupt the immune homeostasis of brain-resident glial cells through cell-type-specific mechanisms, highlighting a potential neurotoxic risk associated with nanoparticulate plastic exposure.

Keywords: Microplastics; Microglia; Astrocyte; Glial activation

INTRODUCTION

The exponential rise in global plastic production since the 1960s has driven widespread environmental contamination (Geyer et al., 2017), particularly from microplastics (<5 mm) and nanoplastics (<1 μm), which originate from the fragmentation of larger plastic material (Kershaw & Rochman, 2015). These particles infiltrate the human body through ingestion, inhalation, and dermal contact (Domenech & Marcos, 2021), with an estimated intake reaching approximately 5 g per week (Senathirajah et al., 2021). Mounting evidence indicates that micro- and nanoplastics are retained in multiple human organs (Jenner et al., 2022; Leslie et al., 2022; Nihart et al., 2025; Øzsoy et al., 2024; Ragusa et al., 2021), raising serious concerns regarding their potential health effects. Notably, studies have identified microplastic deposition in the brain from embryonic stages through adulthood (Amato-Lourenço et al., 2024; Kaur et al., 2024; Shin et al., 2023), with elevated levels detected in individuals with dementia (Nihart et al., 2025). Although the precise mechanisms governing cerebral translocation remain incompletely defined, animal models suggest that microplastics may enter the brain through a compromised blood-brain barrier (BBB) via olfactory and blood vessels (Kaushik et al., 2024; Kopatz et al., 2023). Moreover, microplastics have been implicated in structural and functional disruption of the BBB, along with demyelination and neuroinflammation, which are pathological features of neurodegenerative disease (Nihart et al., 2025). Within the central nervous system (CNS), microglia can internalize microplastics through phagocytosis, triggering alterations in apoptotic signaling pathways and proinflammatory cytokine expression, thereby contributing to microplastic-induced neuroinflammatory processes (Kwon et al., 2022).

Immune surveillance and response within the CNS are primarily orchestrated by microglia and astrocytes, principal resident immune cells that modulate inflammatory signaling,

Received: 06 June 2025; Accepted: 23 October 2025; Online: 24 October 2025

Foundation items: This study was supported by the National Research Foundation of Korea (NRF) funded by the Korean Government (MSIT) (2021R1C1C100328611) and Global-Learning & Academic Research Institution for Master's·PhD students, and Postdocs (G-LAMP) Program of the National Research Foundation of Korea (NRF) funded by the Ministry of Education (RS-2023-00301938)

*Corresponding author, E-mail: jungem@pusan.ac.kr

cytokine and chemokine release, and reactive oxygen species (ROS) generation (Ransohoff & Brown, 2012; Tohidpour et al., 2017). Microglia continuously monitor their microenvironment and dynamically adapt their morphology and functional state in response to perturbations (Gao et al., 2023). These cells are essential for maintaining brain homeostasis, engaging in pathogen recognition, phagocytosis, and immune regulation. During early development, microglia also function as immune sensors of environmental cues, coordinating neurodevelopment by facilitating synaptic pruning and modulation of neuronal circuitry (Thion & Garel, 2017; Xu et al., 2024). However, hyperactivation of microglia can drive maladaptive immune responses, prompting the recruitment of peripheral immune cells and disrupting normal brain development (Chhatbar & Prinz, 2021; Xu et al., 2020), ultimately contributing to the pathogenesis of various neurodegenerative diseases (Butovsky & Weiner, 2018; Hickman et al., 2018).

Astrocytes likewise play multifaceted roles in the CNS, including regulation of synaptic activity, maintenance of homeostasis, modulation of innate immune signaling, and participation in phagocytic clearance (Galloway et al., 2019; Konishi et al., 2022). These cells engage in crosstalk with microglia to regulate inflammation during brain development, preventing impairment of neural maturation due to aberrant immune activity (Panchenko et al., 2023; Zhao et al., 2024). They are also involved in the formation and maintenance of the BBB, a critical interface for neuroprotection from pathogens and toxins (Cabezas et al., 2014). Despite the central roles of microglia and astrocytes in regulating CNS immune dynamics, the impact of microplastic exposure on their immunological function remains unclear. Accumulating evidence indicates that microplastics accumulate in the brain and intensify neuropathological conditions, highlighting the importance of their interactions with brain-resident immune cells.

This study hypothesized that prenatal exposure to polystyrene nanoparticles (PSNs) disrupts neuroimmune function later in life. *In vitro* analyses were performed to identify brain cell types that internalize PSNs and to assess their immune responses following lipopolysaccharide (LPS) stimulation. In parallel, a chronic *in vivo* exposure model was employed in which mice were exposed to PSNs from the fetal stage to adulthood. Results demonstrated that PSNs induced abnormal activation patterns in both microglia and astrocytes, implicating long-term plastic nanoparticle exposure as a potential contributor to neuroimmune dysregulation.

MATERIALS AND METHODS

PSNs

Two types of polystyrene nanoparticles were utilized, including Dragon Green fluorescent polystyrene microspheres (cat. No. FSDG002, 0.20 μm) and non-functionalized polystyrene microspheres (cat. No. PS02001, 0.025 μm), both purchased from Bangs Laboratories (Fishers, USA). Fluorescently labeled plastics enabled visualization of PSN behavior, while a mixture of both variants was used in all experimental conditions. Prior to use, PSNs were centrifuged at 13 000 r/min for 15 min at 4°C to remove detergent residues present in the liquid phase, washed twice in ultrapure water, and resuspended in sterile water.

Primary cortical neuron culture

Primary cortical neurons were established following previously described protocols (Jung et al., 2017). Pregnant female mice were euthanized, and primary cortices were collected from embryos on embryonic day 15.5 (E15.5). Tissue dissociation was performed using trypsin (Welgene, Korea), and neurons were seeded at a density of 1×10^5 cells/well in 24-well plates pre-coated with poly-D-lysine and laminin (both from Sigma-Aldrich, USA). Cultures were maintained in neurobasal medium (Gibco, USA) supplemented with 1% N2 (Gibco, USA), 2% B27 (Gibco, USA), 2% L-glutamine (Gibco, USA), and 1% penicillin/streptomycin (Welgene , Korea). Cells were incubated in a humidified incubator at 37°C with 5% CO_2. The day of plating was designated as day 0 *in vitro* (DIV 0). To investigate PSN accumulation, cells were treated with 10 mg/L PSNs on DIV 4 and harvested on DIV 6. Imaging was performed using differential interference contrast and Thunder Imager 3D microscopy (Leica Microsystems, Germany).

Mixed glial cell culture and microglial and astrocyte isolation

Primary mixed glial cultures were prepared from postnatal day 1–3 (P1–3) mice, as described previously (Lee et al., 2024). Following trypsin digestion, single-cell suspensions were cultured in poly-D-lysine-coated T-75 flasks in Dulbecco's Modified Eagle Medium (Gibco, USA) supplemented with 10% fetal bovine serum (Welgene, Korea) and 1% penicillin/streptomycin.

Microglial cells were isolated on DIV 10 by gentle shaking at 180 r/min and 37°C for 1 h. Detached microglia were collected by centrifugation at 1 000 r/min for 5 min at room temperature and resuspended in fresh medium. To isolate astrocytes, remaining adherent cells were gently shaken at 240 r/min and 37°C for 6 h to remove oligodendrocyte precursor cells. The supernatant was discarded, the astrocytes were enzymatically detached from the flask using trypsin, collected by centrifugation at 1 000 r/min for 5 min at room temperature, and resuspended in fresh culture medium. The isolated microglia and astrocytes were seeded into poly-D-lysine-coated 24-well plates at 1×10^5 cells/well for apoptosis assays or 2×10^5 cells/well for morphological analysis. Cultures were maintained under standard incubation conditions in a humidified incubator at 37°C with 5% CO_2. For nanoparticle uptake studies, cells were treated with 10 mg/L PSNs on DIV 1 and harvested on DIV 3 (Supplementary Figure S1).

To model immune activation and assess morphological and functional alterations in PSN-treated glial cells, LPS was applied as a proinflammatory stimulus (Chaiwut & Kasinrerk, 2022; Luo et al., 2025). Both microglia and astrocytes undergo pronounced morphological remodeling within 24 h of LPS exposure (Cheng et al., 2023; He et al., 2021). These early changes are reliably detectable on DIV 3, making it an optimal time point to assess reactive glial phenotypes. For morphological analysis and apoptosis assays, cells were treated with 10 mg/L PSNs on DIV 1 and 10 ng/mL LPS (Sigma-Aldrich, USA) on DIV 2 and harvested on DIV 3. This LPS concentration was selected based on prior evidence demonstrating robust proinflammatory activation without toxicity to microglia (Lively & Schlichter, 2018).

In the present study, "immune response" encompassed both morphological alterations and functional changes in microglia and astrocytes in response to various stimuli. Specifically, microglial activation was assessed from a resting, branched

state to an activated, amoeboid form, while astrocyte transformation was characterized by hypertrophy and glial scar formation. Additionally, cytokine and chemokine production, including interleukin (IL)-1β, tumor necrosis factor (TNF)-α, and IL-6, was evaluated as key mediators of CNS inflammation (Goshi et al., 2025; Tanaka et al., 2014).

Mice

Specific pathogen-free C57BL/6J mice (8 weeks old, 25–30 g) were obtained from Samtaco (Osan, Korea) and maintained in group-housed cages at 22±1°C with 40%–60% relative humidity under a 12 h/12 h light/dark cycle. Following acclimatization, females were mated with males at a 2:1 ratio overnight. Detection of a vaginal plug was designated as E0.5. Pregnant mice were randomly divided into either a vehicle group (drinking water without PSNs, *n*=2) or a PSN-treated group (drinking water containing a mixture of non-fluorescent and fluorescent PSNs at 10 mg/L, *n*=2). Exposure commenced at E9.5 and continued until P28 via oral administration in drinking water. The selected PSN dose has previously been shown not to induce apoptosis in fetal or adult murine brains (Shin et al., 2023). After weaning, female and male offspring mice were separated into two treatment groups: vehicle (*n*=19; ten males, nine females) and PSN-exposed (*n*=15; seven males, eight females). Mice were housed in groups of 3–5 and administered PSNs via drinking water until P63. Body weights were recorded weekly, and behavioral testing was performed on P42 (Supplementary Figure S2). To assess PSN effects on immune reactivity, mice were administered LPS (2 mg/kg in saline) via intraperitoneal injection for three consecutive days before sacrifice. On the final day, mice were treated with LPS 4 h before sacrifice. The LPS dose was selected as the optimal concentration based on previous studies (Da Silva et al., 2024; Lee et al., 2024). Preliminary analyses revealed no sex-dependent differences in PSN-induced responses (Supplementary Figure S3); therefore, data from both sexes were pooled for downstream analyses.

Adult mice consumed water containing 10 mg/L PSNs throughout the exposure period. Assuming an average water intake of 4 mL/day, the resulting PSN ingestion rate was approximately 0.04 mg/day, equating to 2 mg/kg/day for a 0.02 kg mouse. This intake level aligns with human exposure estimates, which range from 0.1 to 5 g/week, corresponding to 0.2–11.7 mg/kg/day for a 60 kg adult (Senathirajah et al., 2021). Accordingly, the experimental concentration used here approximates environmentally relevant human exposure levels (Pham et al., 2023; Senathirajah et al., 2021).

All experimental protocols were approved by the Institutional Animal Care and Use Committee of Pusan National University (protocol code: PNU-2024-0331), and were conducted in accordance with the ARRIVE guidelines and the ILAR Guide for the Care and Use of Experimental Animals.

Immunofluorescence staining

Nine-week-old offspring were anesthetized with 2.5% avertin (2,2,2-tribromoethanol and *tert*-amyl alcohol; Sigma-Aldrich, USA) per gram of body weight. Brains were dissected and briefly fixed in 4% paraformaldehyde (Merck, Germany) at 4°C. After 24 h of post-fixation, tissues were embedded and coronally sectioned at 80 μm using a vibratome (SM2010R; Leica Microsystems, Germany). Sections were transferred onto glass slides and preserved in phosphate-buffered saline (PBS; MedChem Express, USA) at 4°C.

Cultured cells and brain sections were fixed in 4% paraformaldehyde and permeabilized with PBS containing Triton X-100 (0.01% for cultured cells and 0.5% for brain tissues; Sigma-Aldrich). Samples were blocked with PBS containing 5% donkey serum (Merck, Germany) and 0.25% Triton X-100 for 1 h, then probed with anti-IBA-1 (1:1500, Wako Pure Chemical Industries, Japan), anti-GFAP (1:500, Abcam, USA), anti-MBP (1:500, Santa Cruz Biotechnology, USA), anti-Olig2 (1:500, Merck, Germany), anti-cleaved caspase-3 (1:400, Cell Signaling Technology, USA), and anti-Ki-67 (1:500, Cell Signaling Technology, USA) primary antibodies at 4°C overnight. After washing, the samples were incubated with Alexa Fluor 594 goat anti-rabbit (1:1 000, Invitrogen, USA), Alexa Fluor 594 goat anti-mouse secondary antibodies (1:1 000, Invitrogen, USA) and Alexa Fluor 594 donkey anti-goat secondary antibodies (1:1 000, Invitrogen, USA) and counterstained with 100 ng/mL 4′,6-diamidino-2-phenylindole (DAPI; Sigma-Aldrich, USA) for 1 h. Fluorescently labeled cells were visualized using a Thunder Imager 3D microscope (DMi8; Leica Microsystems, Germany).

Morphological analysis

Morphological analysis was performed as described previously (Lee et al., 2024). For cultured microglia and astrocytes, three to four fields per coverslip were randomly selected and imaged using the Thunder Imager 3D system (DMi8; Leica Microsystems, Germany). For brain tissue, four independent biological replicates per group were processed, and both hemispheres from each animal were imaged. One representative region per hemisphere was selected for quantification. Immunolabeled IBA-1-positive microglia and GFAP-positive astrocytes were counted using ImageJ (NIH, USA). Based on morphology, IBA-1-positive cells were classified into three subtypes: ramified (small somata with multiple fine processes), bushy (enlarged somata with thick processes), and amoeboid-like (rounded cell bodies with few or no processes) as defined by (Wicks et al., 2022). The proportion of each subtype was calculated relative to total microglial counts in each sample. GFAP-positive cells were classified into two subtypes: resting (small cell bodies with minimal branching) and reactive (enlarged cell bodies with extensive branching) (Wilhelmsson et al., 2006). The percentages of resting and reactive astrocytes were calculated and compared across experimental groups.

Quantitative real-time polymerase chain reaction (qPCR)

Gene expression was assessed via qPCR in mice from four treatment groups: vehicle (*n*=6; three males, three females), PSNs (*n*=5; two males, three females), vehicle+LPS (*n*=7; four males, three females), and PSNs+LPS (*n*=6, three males, three females). Animals were euthanized on P63. Total RNA was extracted from whole-brain tissue using Tri-RNA reagent (Favorgen, Taiwan, China) following the manufacturer's protocols, as described previously (Jung et al., 2010). RNA concentrations were quantified using an Epoch microplate spectrophotometer (BioTek, USA), and cDNA was synthesized using M-MLV reverse transcriptase (Invitrogen, USA).

qPCR was performed using SYBR Green chemistry on a QuantStudio 3 system (Applied Biosystems, USA). Thermal cycling conditions were as follows: initial activation of uracil-DNA glycosylase at 50°C for 2 min; uracil-DNA glycosylase inactivation, Hot start Taq DNA polymerase activation, and template denaturation at 95°C for 2 min; and 40 cycles of

95°C for 15 s, 60°C for 15 s, and 72°C for 20 s. After amplification, a melting curve was generated by heating the samples to 95°C for 15 s, followed by cooling down to 60°C for 1 min at 1.6°C/s. Fluorescence was measured continuously while slowly heating to 95°C at 0.15°C/s. *Gapdh* served as an internal control for normalization. Primer sequences are listed in Supplementary Table S1.

Statistical analysis

Sample sizes were determined using G*Power software (Heinrich-Heine-Universität Düsseldorf, Germany) with power=0.85 and alpha=0.05. Data are reported as mean±standard error of the mean (SEM). Means of two independent groups were compared using unpaired Student's *t*-tests, while one-way analysis of variance (ANOVA) with Bonferroni *post-hoc* test was applied for multiple comparisons. Each dataset was assessed for normality testing using the Shapiro-Wilk test and *Q*-*Q* plots (Shapiro & Wilk, 1965). Datasets that satisfied normality assumptions were analyzed using parametric tests. Datasets that did not meet normality criteria were analyzed using nonparametric Mann-Whitney *U* tests (Ghasemi & Zahediasl, 2012). All data were analyzed using GraphPad Prism v.8.0 (GraphPad Software, USA). Statistical significance was set to $P<0.05$. All experiments were independently repeated in triplicate and conducted in a blinded and randomized manner. Animals were randomly assigned to the different experimental groups. Data collection and processing were carried out randomly. Animal treatment, handling, and allocation were consistent across all study groups.

RESULTS

PSNs selectively accumulate in glial cells of the CNS

To determine the cellular specificity of PSN uptake in the CNS, primary cortical neurons and mixed glial cultures were exposed to PSNs *in vitro*. Fluorescent imaging revealed no detectable intracellular PSN accumulation in neurons, whereas substantial uptake occurred in glial cells (Figure 1A). When glial subtypes (microglia, astrocytes, and oligodendrocytes) were cultured separately, PSNs accumulated at higher levels in microglia than in astrocytes, but were absent in oligodendrocytes (Figure 1B–D). Microglia were observed to phagocytose other microglia that had internalized PSNs and undergone apoptosis (Figure 1E). *In vivo* analyses further confirmed PSN accumulation in microglia and astrocytes within the brains of offspring prenatally exposed via maternal ingestion during gestation (Figure 1F, G; Supplementary Figure S4).

PSNs affect the immune response in LPS-treated primary microglial cells and astrocytes

To assess the immunomodulatory effects of PSNs, microglia and astrocytes were sequentially treated with PSNs followed by LPS stimulation, and their activation states were evaluated morphologically. Microglia exhibit distinct morphological features depending on their activation level. The ramified state is the resting and homeostatic form, whereas the bushy and amoeboid states represent increasingly activated forms involved in immune responses, with the amoeboid state being the most reactive and inflammatory (Vidal-Itriago et al., 2022). Similarly, astrocytes undergo morphological changes upon activation (Zhou et al., 2019).

Microglia were isolated, cultured, and sequentially treated with PSNs and LPS (24 h after PSN treatment). Microglia were immunolabeled with IBA-1, a specific microglia marker, and categorized into ramified, bushy, or amoeboid morphologies, representing resting, moderately activated, and highly reactive states, respectively (Figure 2A). LPS treatment increased microglial numbers in both vehicle and PSN-exposed cultures (Figure 2B). Although the PSN+LPS group exhibited a greater increase in cell number than the vehicle+LPS group, the difference was not statistically significant. Ramified microglia were more prevalent in the untreated vehicle group compared to all other conditions (Figure 2C). Exposure to PSNs alone significantly increased the proportion of activated morphologies, and combined PSN+LPS treatment further amplified the frequency of amoeboid microglia relative to LPS alone.

Astrocytes were similarly evaluated following sequential exposure to PSNs and LPS. GFAP immunostaining was used to quantify reactive and resting astrocytes and assess morphological changes (Figure 2D). The number of GFAP-positive cells was significantly higher in the PSN group compared with the vehicle group, whereas no significant difference was observed between the LPS-treated vehicle and PSN groups (Figure 2E). LPS stimulation reduced the proportion of resting astrocytes while increasing reactive astrocyte prevalence in the vehicle group. However, astrocytes in the PSN+LPS group exhibited a smaller shift towards the reactive phenotype than those in the vehicle+LPS group (Figure 2F). Taken together, these results suggest that PSNs may differentially influence the activation of microglia and astrocytes, likely through distinct regulatory mechanisms.

PSNs affect apoptosis in LPS-treated primary microglia and astrocytes

Apoptosis plays a central role in regulating cellular responses to inflammatory stimuli (Haanen & Vermes, 1995). In particular, microglial overactivation has been linked to apoptotic death, characterized by DNA fragmentation and caspase-3 activation (Liu et al., 2001). To investigate whether PSNs modulate glial cell apoptosis during neuroinflammatory challenge, primary microglia and astrocytes were sequentially treated with PSNs and LPS, followed by immunofluorescence staining for cleaved caspase-3, a key effector of apoptosis (Figure 3A, C). In microglia, LPS exposure significantly reduced cleaved caspase-3 expression in both vehicle- and PSN-treated groups, indicating decreased apoptotic signaling in response to inflammatory activation (Figure 3B). Notably, cleaved caspase-3 levels were lower in PSN-treated microglia than in vehicle-treated controls, regardless of LPS treatment. In contrast, astrocytes exhibited elevated cleaved caspase-3 expression following both PSN and LPS treatment compared to the vehicle treatment (Figure 3D). In PSN-treated astrocytes, the increase in cleaved caspase-3 expression following LPS treatment was not statistically significant, suggesting a weaker apoptotic response than that observed in the vehicle group. Collectively, these findings indicate that PSNs exert distinct regulatory effects on apoptosis in microglia and astrocytes in the context of neuroinflammation.

PSNs affect microglial responses in LPS-treated mice

To investigate whether developmental exposure to PSNs alters microglial responses in later life, pregnant mice were administered PSNs beginning at E9.5, a time point corresponding to the onset of neurogenesis, and treatment was continued through weaning (Bani-Yaghoub et al., 2006;

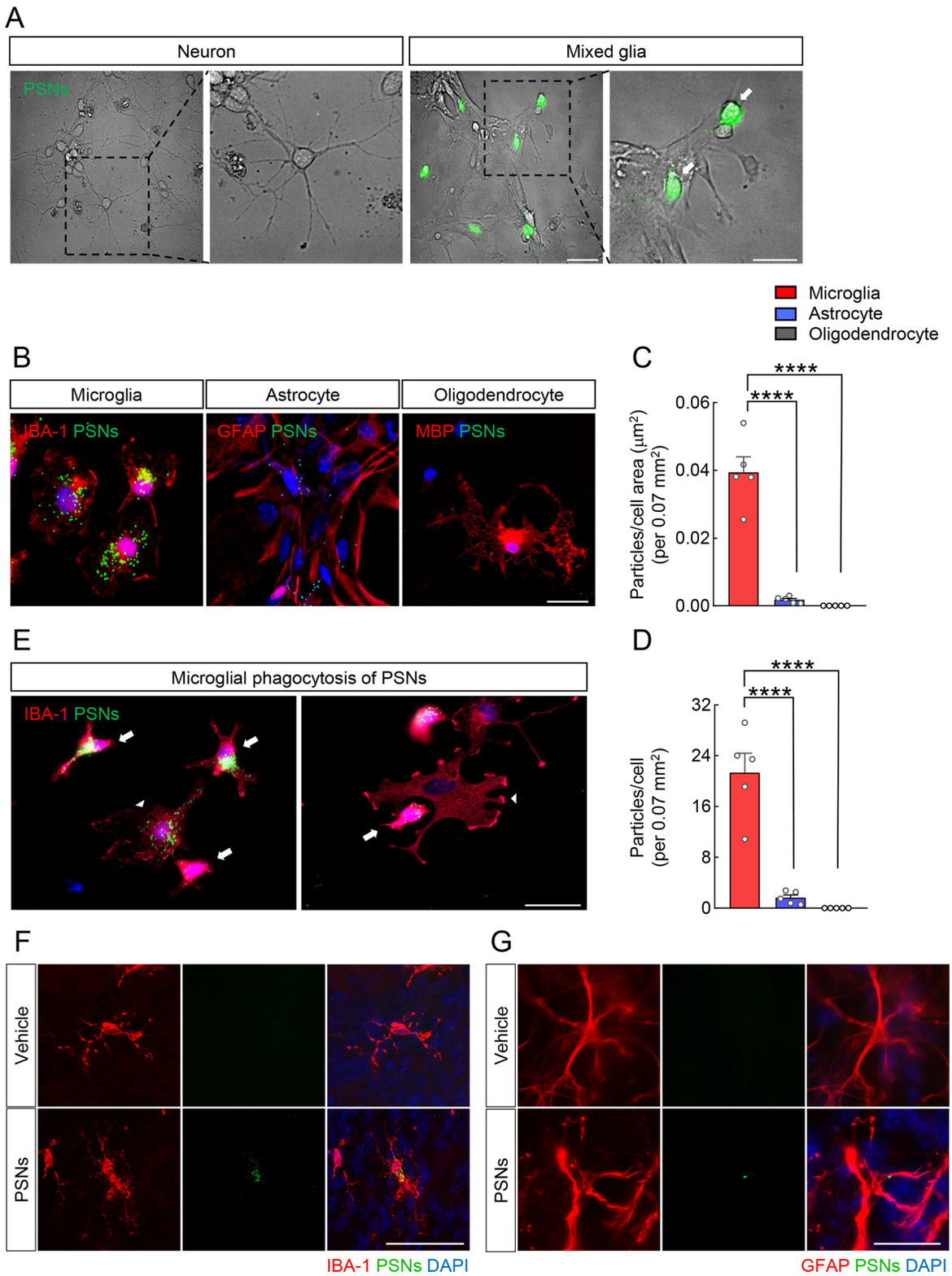

Figure 1 PSNs are internalized by mixed glial cells, particularly microglia and astrocytes, *in vitro* and *in vivo*

A: Differential interference contrast and magnified images of neurons and mixed glial cells. PSNs are labeled with a white arrow. Scale bars: 50 μm and 30 μm (for magnified views). B: Representative images of primary glial cells (microglia, astrocytes, and oligodendrocytes). Scale bar: 30 μm. C: Quantitative analysis of PSN accumulation rate based on cell area. Microglia vs. astrocytes, ****: P<0.0001; microglia vs. oligodendrocytes, ****: P<0.0001 (one-way ANOVA with Bonferroni correction). D: Quantitative analysis of PSN accumulation rate based on cell number. n=3 cell cultures repeated using three mice. Microglia vs. astrocytes, ****: P<0.0001; microglia vs. oligodendrocytes, ****: P<0.0001 (one-way ANOVA with Bonferroni correction). E: Images showing PSN-loaded microglia undergoing apoptosis, labeled with white arrows, and PSN-loaded dead microglia being phagocytosed by other microglia, labeled with white arrowheads. Scale bar: 25 μm. F: Representative images showing IBA-1- (red) and DAPI (blue)-stained microglial cells in P1 mouse brain. Scale bar: 50 μm. G: Representative images showing GFAP- (red) and DAPI (blue)-stained astrocytes in P1 mouse brain. Scale bar: 50 μm. Data are presented as mean±SEM.

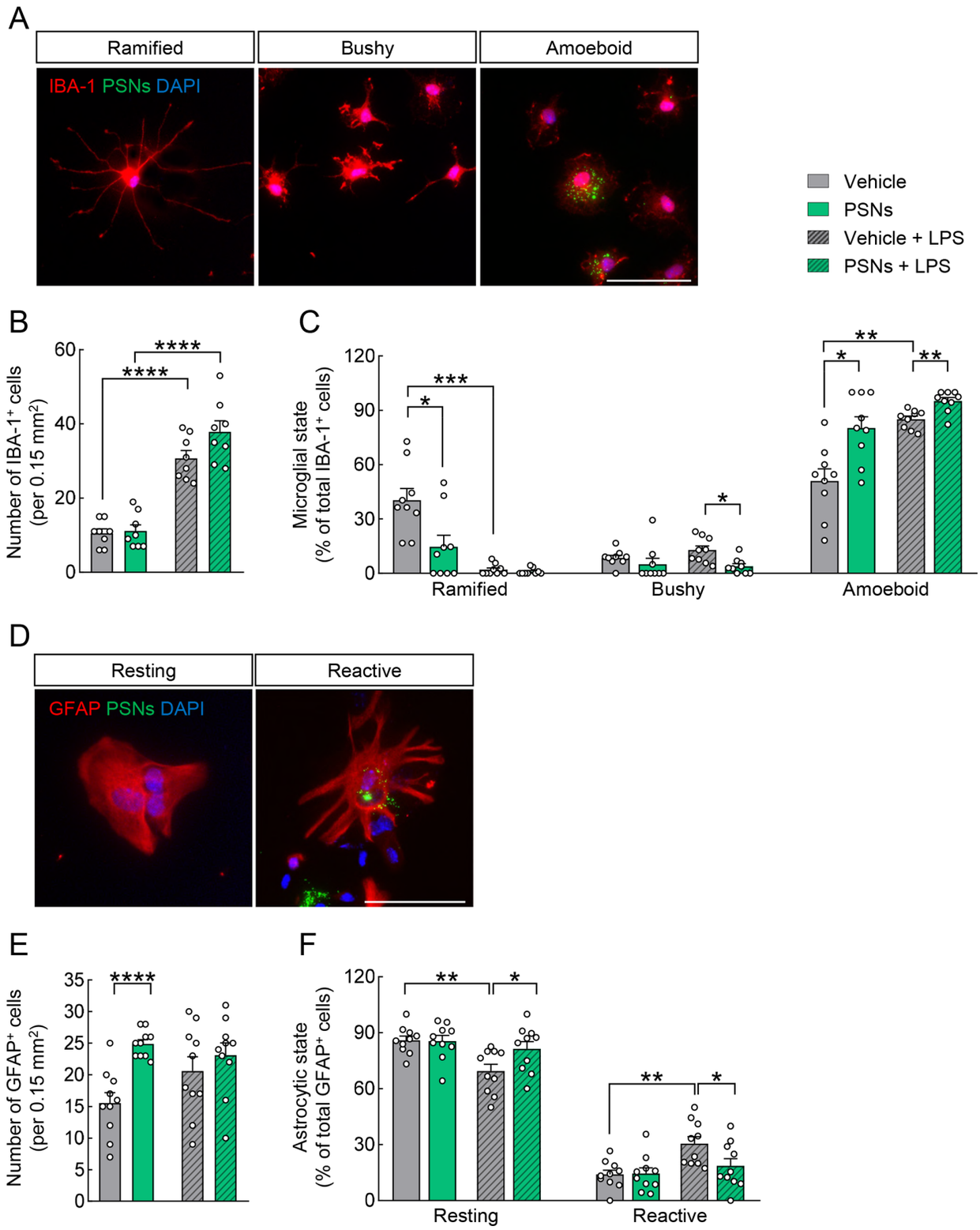

Figure 2 PSNs promote microglial activation and suppress astrocytic activation

A: Representative images showing IBA-1- (red) and DAPI (blue)-stained primary microglial cells. Scale bar: 50 μm. B: Quantitative analysis of IBA-1-positive cells. Vehicle vs. vehicle+LPS, P<0.0001; PSNs vs. PSNs+LPS, P<0.0001 (two-tailed Student's t-test). C: Quantitative analysis of microglial state transition rate. n=3 cell cultures repeated using three mice. Ramified: vehicle vs. PSNs, P=0.0258; vehicle vs. vehicle+LPS, P=0.0002; bushy: vehicle+LPS vs. PSNs+LPS, P=0.0103; amoeboid: vehicle vs. PSNs, P=0.019; vehicle vs. vehicle+LPS, P=0.0011; vehicle+LPS vs. PSNs+LPS, P=0.007 (Mann-Whitney U test). D: Representative images showing GFAP- (red) and DAPI (blue)-stained primary astrocytes. Scale bar: 100 μm. E: Quantitative analysis of GFAP-positive cells. Vehicle vs. PSNs, P<0.0001 (two-tailed Student's t-test). F: Quantitative analysis of astrocytic state transition rates. n=3 cell cultures repeated using three mice. Resting: vehicle vs. vehicle+LPS, P=0.0014; vehicle+LPS vs. PSNs+LPS, P=0.041; reactive: vehicle vs. vehicle+LPS, P=0.0014; vehicle+LPS vs. PSNs+LPS, P=0.041 (two-tailed Student's t-test). Data represent mean±SEM. *: P<0.05; **: P<0.01; ***: P<0.001; ****: P<0.0001.

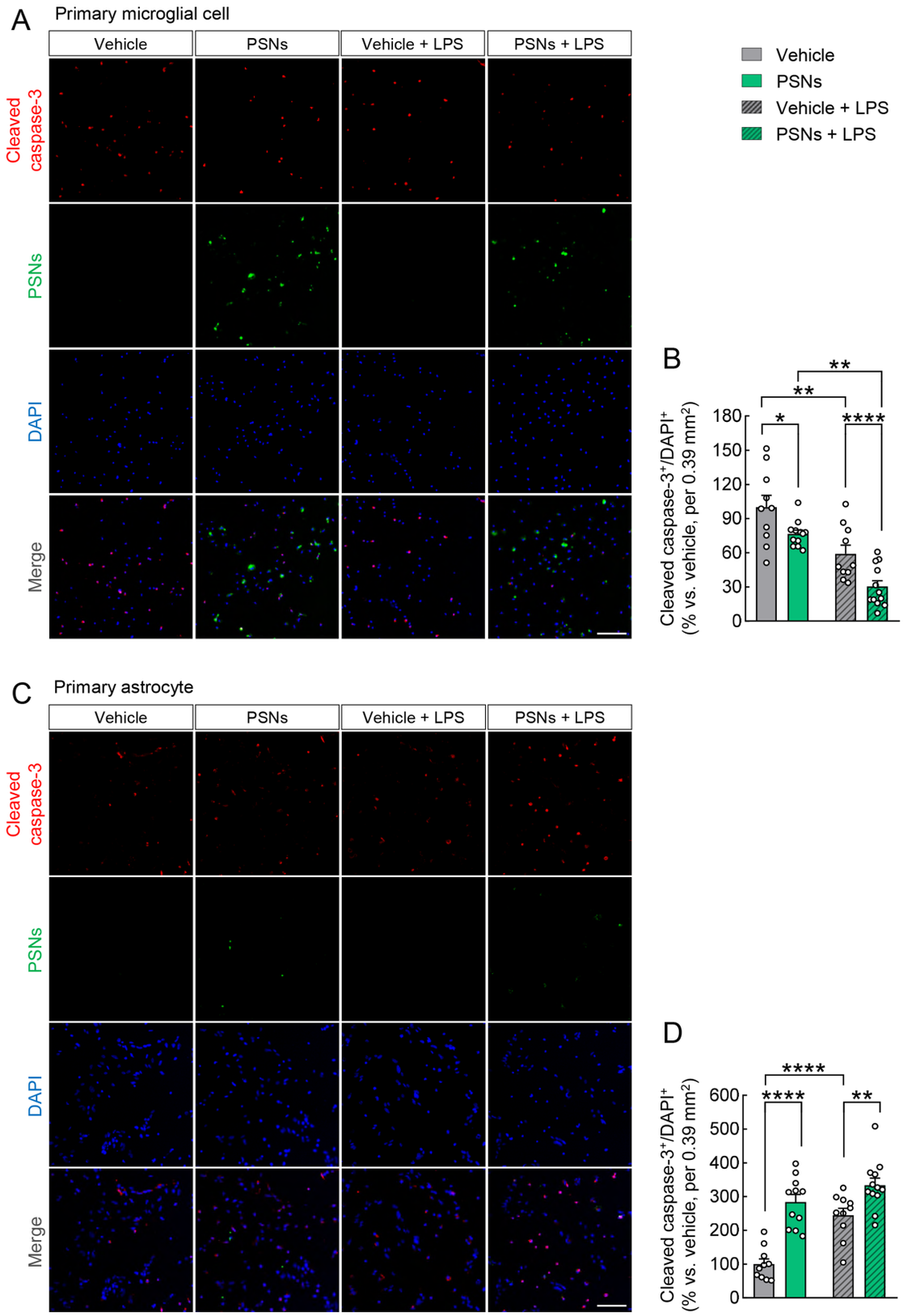

Figure 3 PSNs suppress microglial apoptosis but induce astrocytic apoptosis, exerting stronger effects than LPS

A: Representative image of primary microglia stained for cleaved caspase-3 (red) and counterstained with DAPI (blue). Scale bar: 100 μm. B: Quantitative analysis of apoptosis relative to that in vehicle group, with cleaved caspase-3$^+$/DAPI$^+$ set to 100%. n=3 cell cultures repeated using three mice. Vehicle vs. PSNs, P=0.0306; vehicle vs. vehicle+LPS, P=0.0052; PSNs vs. PSNs+LPS, P=0.0042; vehicle+LPS vs. PSNs+LPS, P<0.0001 (two-tailed Student's t-test). C: Representative image of primary astrocytes stained for cleaved caspase-3 (red) and counterstained with DAPI (blue). Scale bar: 100 μm. D: Quantitative analysis of apoptosis relative to that in vehicle group, with cleaved caspase-3$^+$/DAPI$^+$ set to 100%. n=3 cell cultures repeated using three mice. Vehicle vs. PSNs, P<0.0001; vehicle vs. vehicle+LPS, P<0.0001; vehicle+LPS vs. PSNs+LPS, P=0.0084 (two-tailed Student's t-test). Data represent mean±SEM. *: P<0.05; **: P<0.01; ****: P<0.0001.

Casoni et al., 2024). To evaluate microglial responses to inflammatory challenge, offspring were injected with LPS two days prior to sacrifice, and immunofluorescence staining with IBA-1 was used to quantify microglial number and morphology in the cortex and hippocampus (Figure 4A). These brain regions were selected due to their high susceptibility to neuroinflammation and their abundance of glial populations. The hippocampus, which regulates learning, memory, and emotion, is particularly sensitive to environmental stressors, including microplastic exposure (Paing et al., 2024; Shin et al., 2023), while the cerebral cortex plays a critical role in higher-order brain functions and is frequently implicated in early-stage neurodegenerative and neurodevelopmental pathologies (Li et al., 2022).

In the cortex, LPS treatment led to a significant increase in microglial number in both vehicle- and PSN-exposed mice, indicating microglial activation in response to LPS (Figure 4B). No significant differences in microglial cell counts were observed between vehicle and PSN groups, irrespective of LPS exposure. LPS also induced a significant reduction in the percentage of ramified microglia in both groups (Figure 4C). Interestingly, the vehicle group exhibited a slightly higher proportion of ramified microglia than the PSN group, whereas the vehicle+LPS group displayed a slightly lower proportion of ramified cells than the PSN+LPS group. LPS significantly increased the proportions of bushy and amoeboid cells both treatment groups, with the PSN group showing a higher proportion of bushy cells than vehicle controls.

In the hippocampus, PSN-exposed mice displayed a significantly higher number of microglia than vehicle-treated mice, regardless of LPS stimulation (Figure 4D, E). In both groups, LPS reduced the proportion of ramified cells and increased the proportions of bushy and amoeboid cells (Figure 4F). Notably, following LPS treatment, the PSN group exhibited a significantly higher proportion of bushy cells and a significantly lower proportion of amoeboid cells compared to the vehicle group. These findings suggest that developmental exposure to PSNs alters both the abundance and activation patterns of microglia in response to inflammatory stimuli, with region-specific effects in the cortex and hippocampus.

PSNs alter astrocyte and oligodendrocyte populations in LPS-treated mice

To evaluate the effects of PSNs on astrocytes and oligodendrocytes *in vivo*, cell numbers were quantified in the cortex and hippocampus using GFAP and Olig2 immunolabeling, respectively. In the cortex, astrocyte numbers did not differ significantly across experimental groups (Figure 5A, B). In contrast, the hippocampus showed a modest increase in GFAP-positive cells following LPS or PSN treatment compared to vehicle controls (Figure 5C, D), although PSN+LPS co-treatment did not produce an additional effect. In the cortex, oligodendrocyte counts were reduced after LPS treatment in both vehicle- and PSN-treated mice, whereas no significant difference was observed in the hippocampus (Figure 5F, H). These findings suggest that PSNs can induce astrocytic dysfunction, while exerting limited impact on oligodendrocytes, even in the presence of an inflammatory stimulus.

PSNs affect gene expression in mice

To assess the molecular effects of PSNs on glial activation and neuroinflammation, mRNA expression levels of glial cell markers and cytokines were analyzed in whole-brain tissue from mice treated with PSNs and/or LPS. As a physiological indicator of systemic inflammation, the spleen-to-body weight ratio was significantly elevated in response to LPS treatment in both the vehicle and PSN groups, confirming successful induction of an inflammatory response (Liverani et al., 2014) (Figure 6A–F). The mRNA levels of *Iba-1*, *Gfap*, and transforming growth factor-β1 (*Tgfβ1*) were significantly up-regulated in both the vehicle and PSN groups following LPS treatment (Figure 6G, H, K). Notably, the PSN+LPS group exhibited significantly lower *Iba-1* expression than the vehicle+LPS group. In contrast, the expression of *Olig2* and inflammatory cytokines *Tnfα*, *Il-6*, and *Il-10* did not significantly differ among groups (Figure 6I, J, L, M). These findings indicate that PSNs influence microglia and astrocyte activation at the transcriptional level, particularly in the presence of a potent inflammatory stimulus, but do not broadly alter oligodendrocyte marker expression or overall cytokine output in the brain. This suggests that PSN-induced immune modulation may occur in a cell type- and pathway-specific manner.

DISCUSSION

The present study demonstrated that PSNs preferentially accumulated in glial cells, particularly microglia and astrocytes, both *in vivo* and *in vitro*. Given the central role of these cells in neuroimmune surveillance, their selective uptake of PSNs prompted further investigation into PSN-induced immunomodulation. Notably, PSNs measuring 200 nm were substantially accumulated in primary microglia and to a lesser extent in astrocytes. As the resident macrophage-like cells of the CNS, microglia possess robust phagocytic activity (Fu et al., 2014), enabling efficient uptake of exogenous particles, including synthetic nanoplastics (Kwon et al., 2022). In contrast, astrocytes primarily contribute to neurotransmitter regulation, synaptic maintenance, and metabolic support, with limited phagocytic capacity (Kim et al., 2019; Liu et al., 2021), consistent with the lower PSN accumulation observed. The absence of PSN internalization in neurons and oligodendrocytes may reflect size- and cell type-specific uptake dynamics. Prior studies have shown that polystyrene particles ranging from 50 to 500 nm induce transcriptional and functional alterations predominantly in astrocytes, with minimal effects on neurons and oligodendrocytes, suggesting limited uptake in neuronal lineages (Marcellus et al., 2024). In contrast, other studies have reported that smaller nanoplastics may penetrate neurons via endocytic pathways or affect membrane integrity without internalization (Adamiak et al., 2025; Huang et al., 2023; Kim et al., 2025). Collectively, these findings support the idea that particle size critically modulates intracerebral localization and that harmful effects on neurons may occur through indirect mechanisms, such as glia-mediated inflammatory signaling or membrane interaction, rather than direct accumulation.

Accumulation of PSNs in brain-resident immune cells prompted investigation into their potential to modulate neuroimmune responses. To simulate neuroinflammatory conditions, LPS, a glycolipid component of gram-negative bacterial membranes known to induce robust immune activation (Liu et al., 2024), was employed as an immune stimulus in glial cell cultures and in mice. LPS is a strong immune stimulant, particularly in microglia and astrocytes, two glial populations critical for maintaining CNS homeostasis (Pascual et al., 2012). Although LPS does not readily cross

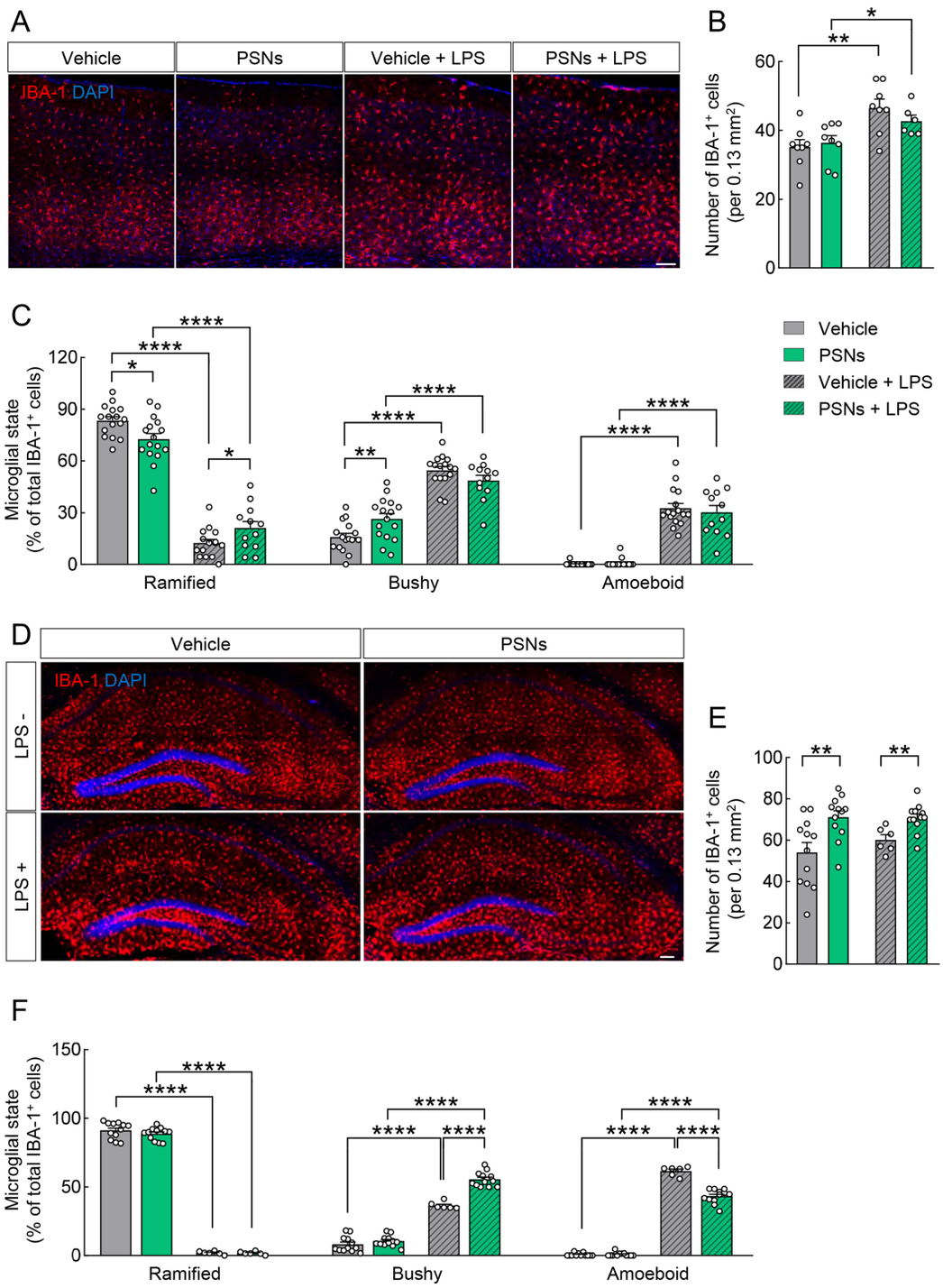

Figure 4 PSNs increase microglial cell number, particularly in the hippocampus, in adult mice

A: Representative fluorescence images of cortical region in vehicle- and PSN+LPS-treated mouse brains stained for IBA-1 (red) and counterstained with DAPI (blue). Scale bar: 100 μm. B: Quantitative analysis of IBA-1-positive cells. Vehicle vs. vehicle+LPS, P=0.0043, PSNs vs. PSNs+LPS, P=0.0489 (two-tailed Student's t-test). C: Quantitative analysis of microglial state rate. n=2 (one male, one female) for vehicle, n=2 (one male, one female) for PSNs, n=2 (one male, one female) for vehicle+LPS, n=2 (one male, one female) for PSNs+LPS. Ramified: vehicle vs. PSNs, P=0.0112; vehicle vs. vehicle+LPS, P<0.0001; PSNs vs. PSNs+LPS, P<0.0001; vehicle+LPS vs. PSNs+LPS, P=0.0412; bushy: vehicle vs. PSNs, P=0.0076; vehicle vs. vehicle+LPS, P<0.0001; PSNs vs. PSNs+LPS, P<0.0001; amoeboid: vehicle vs. vehicle+LPS, P<0.0001; PSNs vs. PSNs+LPS, P<0.0001 (two-tailed Student's t-test). D: Representative fluorescence images of hippocampal region in vehicle- and PSN+LPS-treated mouse brains stained for IBA-1 (red) and counterstained with DAPI (blue). Scale bar: 100 μm. E: Quantitative analysis of IBA-1-positive cells. Vehicle vs. vehicle+LPS, P=0.0064, vehicle+LPS vs. PSNs+LPS, P=0.0061 (two-tailed Student's t-test). F: Quantitative analysis of IBA-1-positive cells. n=2 (one male, one female) for vehicle, n=2 (one male, one female) for PSNs, n=2 (one male, one female) for vehicle+LPS, n=2 (one male, one female) for PSNs+LPS. Ramified: vehicle vs. vehicle+LPS, P<0.0001; PSNs vs. PSNs+LPS, P<0.0001; bushy: vehicle vs. vehicle+LPS, P<0.0001; PSNs vs. PSNs+LPS, P<0.0001; vehicle+LPS vs. PSNs+LPS, P<0.0001; amoeboid: vehicle vs. vehicle+LPS, P<0.0001; PSNs vs. PSNs+LPS, P<0.0001; vehicle+LPS vs. PSNs+LPS, P<0.0001 (two-tailed Student's t-test). Data represent mean±SEM. *: P<0.05; **: P<0.01; ****: P<0.0001.

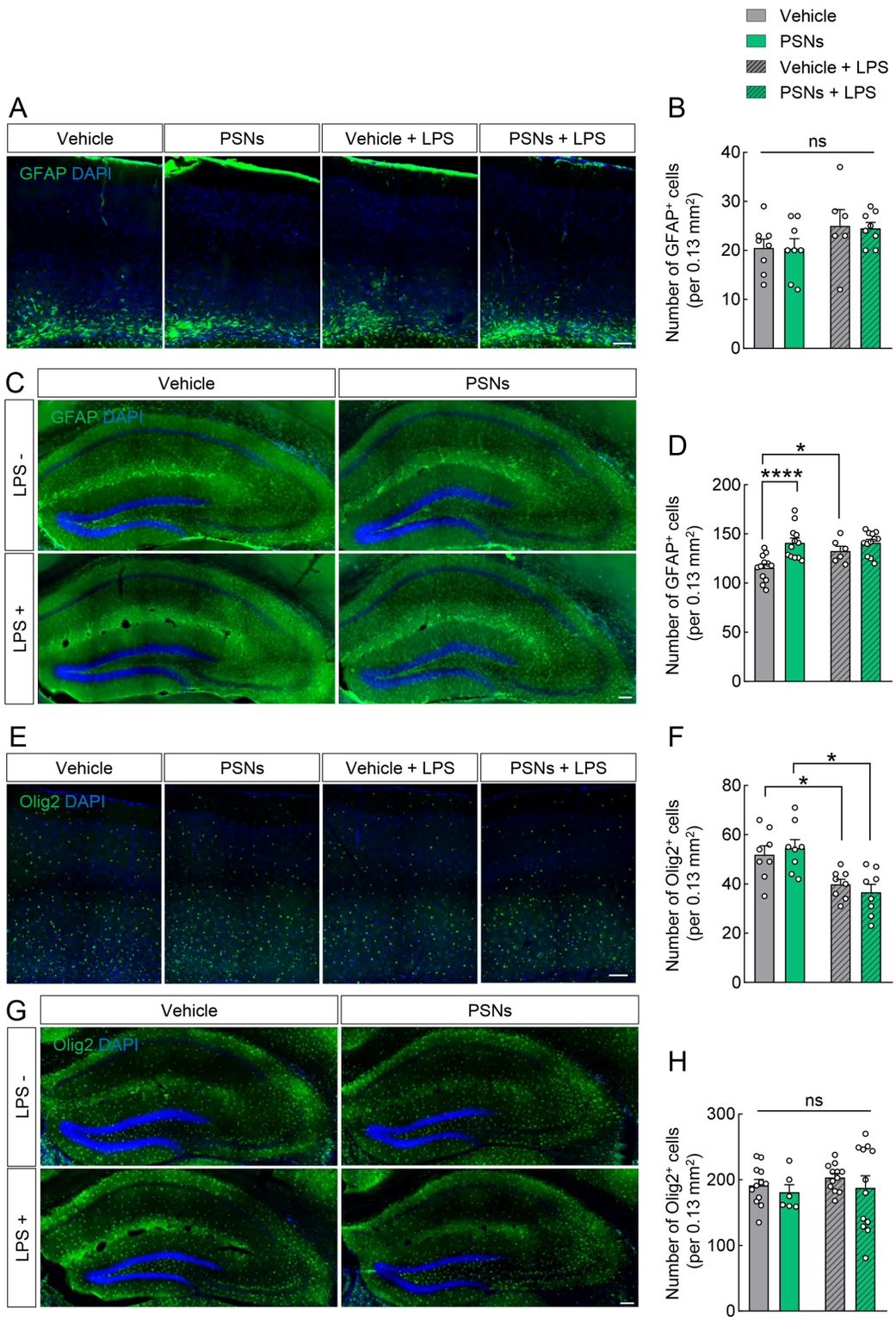

Figure 5 PSNs exert no notable effect on LPS-induced immune responses in oligodendrocytes

A: Representative fluorescence images of cortical region in vehicle- and PSN+LPS-treated mouse brains stained for GFAP (green) and counterstained with DAPI (blue). Scale bar: 100 μm. B: Quantitative analysis of GFAP-positive cells. C: Representative fluorescence images of hippocampal region in vehicle- and PSN+LPS-treated mouse brains stained for GFAP (green) and counterstained with DAPI (blue). Scale bar: 100 μm. D: Quantitative analysis of GFAP-positive cells. Vehicle vs. PSNs, P<0.0001; vehicle vs. vehicle+LPS, P=0.0176 (two-tailed Student's t-test). E: Representative fluorescence images of cortical region in vehicle- and PSN+LPS-treated mouse brains stained for Olig2 (green) and counterstained with DAPI (blue). Scale bar: 100 μm. F: Quantitative analysis of Olig2-positive cells. n=2 (one male, one female) for vehicle, n=2 (one male, one female) for PSNs, n=2 (one male, one female) for vehicle+LPS, n=2 (one male, one female) for PSNs+LPS. Vehicle vs. vehicle+LPS, P=0.0116; PSNs vs. PSNs+LPS, P=0.0024 (two-tailed Student's t-test). G: Representative fluorescence images of hippocampal region in vehicle- and PSN+LPS-treated mouse brains stained for Olig2 (green) and counterstained with DAPI (blue). Scale bar: 100 μm. H: Quantitative analysis of Olig2-positive cells. Data represent mean±SEM. *: P<0.05; ****: P<0.0001; ns: Not significant.

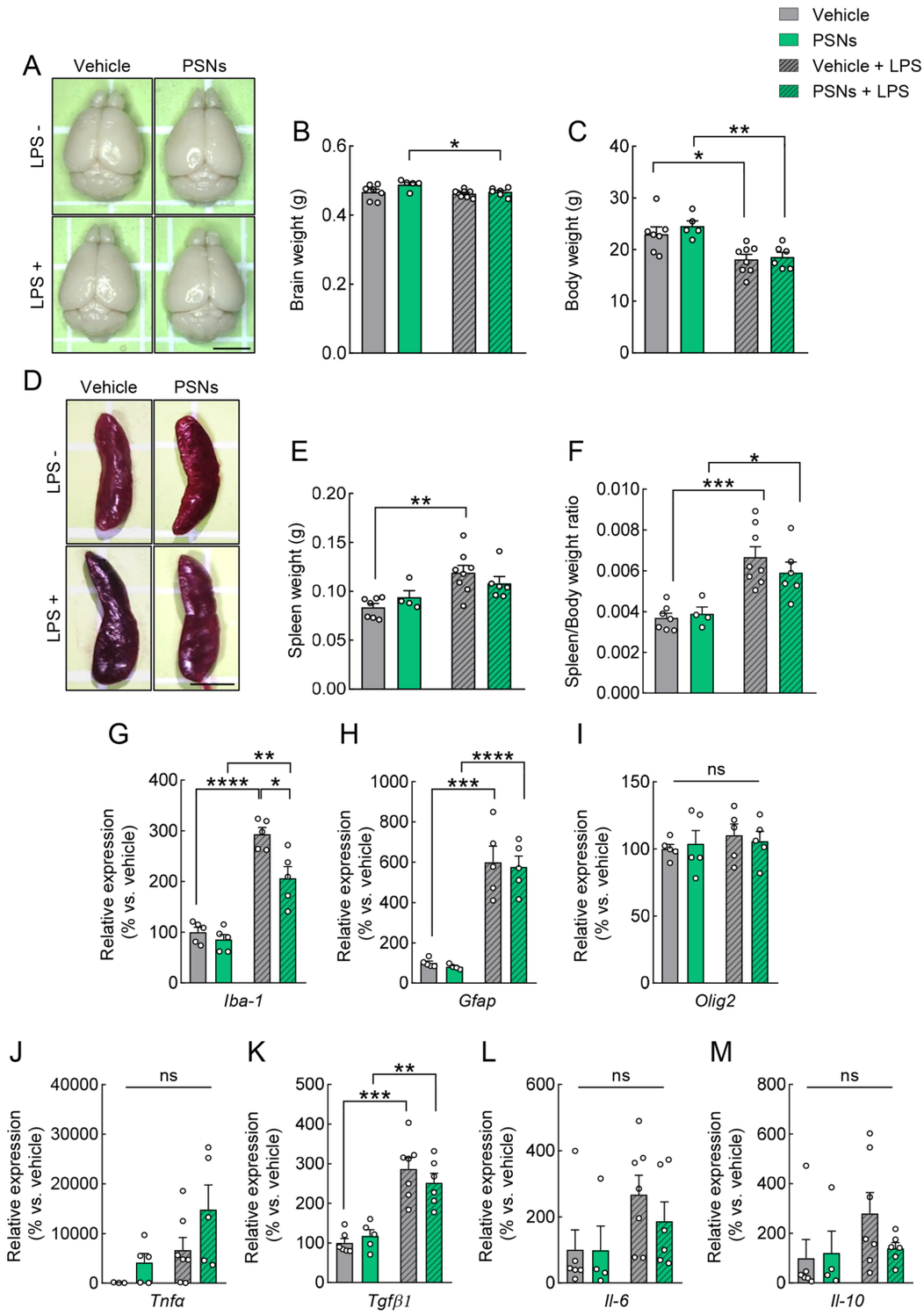

Figure 6 Quantitative analysis of genes encoding glial cell markers and several cytokines

A: Representative images of the brains of 9-week-old mice treated with vehicle or PSNs and LPS. Scale bar: 0.5 cm. B: Brain weight. PSNs vs. PSNs+LPS, P=0.0271 (two-tailed Student's t-test). C: Body weight. Vehicle vs. vehicle+LPS, P=0.0107; PSNs vs. PSNs+LPS, P=0.0019 (two-tailed Student's t-test). D: Representative images of spleens from vehicle or PSN- and LPS-treated mice. Scale bar: 0.5 cm. E: Spleen weight. Vehicle vs. vehicle+LPS, P=0.0017 (two-tailed Student's t-test). F: Spleen-body weight ratio. n=6 (three males, three females) for vehicle, n=5 (two males, three females) for PSNs, n=7 (four males, three females) for vehicle+LPS, n=6 (three males, three females) for PSNs+LPS. Vehicle vs. vehicle+LPS, P=0.0002; PSNs vs. PSNs+LPS, P=0.0208 (two-tailed Student's t-test). Gene expression was normalized to *Gapdh*. G: *Iba-1* expression: vehicle vs. vehicle+LPS, P<0.0001; PSNs vs. PSNs+LPS, P=0.0014; vehicle+LPS vs. PSNs+LPS, P=0.0113. H: *Gfap* expression: vehicle vs. vehicle+LPS, P=0.0002; PSNs vs. PSNs+LPS, P<0.0001. I: *Olig2* expression. J: *Tnfα* expression. K: *Tgfβ1* expression: vehicle vs. vehicle+LPS, P=0.0001; PSNs vs. PSNs+LPS, P=0.0016. L: *Il-6* expression. M: *Il-10* expression. n=6 (three males, three females) for vehicle, n=5 (two males, three females) for PSNs, n=7 (four males, three females) for vehicle+LPS, n=6 (three males, three females) for PSNs+LPS; two-tailed Student's t-test. Data represent mean±SEM of triplicate experiments. *: P<0.05; **: P<0.01; ***: P<0.001; ****: P<0.0001; ns: Not significant.

the BBB, it compromises barrier integrity and initiates neuroinflammation by engaging Toll-like receptor 4 on vascular endothelial cells and microglia, as well as through peripheral inflammatory signaling (Haruwaka et al., 2019; He et al., 2021). These responses closely mimic the cellular and molecular features of CNS inflammation, making LPS a suitable model for studying neuroimmune activation. Systemically, LPS-induced splenomegaly (spleen enlargement) has been observed upon co-treatment with PSNs and LPS and can be interpreted as an inflammatory response marker (Liverani et al., 2014). This model thus provides a platform to assess how PSNs influence glial reactivity under inflammatory conditions.

Under inflammatory conditions *in vitro*, PSNs promoted LPS-induced microglial cell activation while attenuating reactive transformation of astrocytes. These distinct immune responses of microglia and astrocytes underscore a cell type-specific modulatory effect of PSNs on neuroimmune function. However, *in vivo* analyses revealed minimal PSN-mediated alterations in glial activation. This discrepancy likely stems from differences in microenvironmental context. In primary cultures, the absence of a BBB permits direct PSN-glia interactions and amplifies LPS responsiveness. In contrast, the intact BBB *in vivo* restricts PSN penetration into the parenchyma, limiting their immunomodulatory capacity (Tran et al., 2022)(Asimakidou et al., 2024). Consequently, the apparent potency of PSNs observed *in vitro* may reflect artificial exposure conditions not representative of physiological barriers. This may explain why PSNs had less pronounced effects on the brain immune system than in the *in vitro* model. Therefore, the apparent effectiveness of PSNs in the *in vitro* experiments is likely because of the direct interaction between PSNs and immune cells in the absence of the BBB.

PSNs induced pronounced morphological and functional activation of microglia *in vitro*, promoting a transition from surveillant to bushy and amoeboid phenotypes. The bushy state represents partial activation with limited mobility, characteristic of early immune responses (Ziebell et al., 2015), while the amoeboid form denotes full activation, marked by elevated cytokine secretion, phagocytic capacity, and migratory behavior (Ziebell et al., 2015). Exposure to PSNs increased the proportion of microglia exhibiting the amoeboid phenotype, an effect further amplified in the presence of LPS, indicating a synergistic enhancement of proinflammatory activation. PSN exposure also suppressed microglial apoptosis, and when combined with LPS, resulted in a significant increase in microglial cell numbers alongside further reductions in apoptosis, suggesting prolonged survival of activated microglia and potential amplification of neuroinflammatory responses (Gao et al., 2023). Morphological analysis revealed that LPS robustly activated astrocytes, whereas PSN exposure tended to reduce LPS-induced astrocyte activation *in vitro*. Interestingly, PSNs significantly enhanced astrocyte apoptosis, particularly when combined with LPS. In kidney cells, co-treatment with PSNs and LPS induced excessive ROS production in cells, driving oxidative stress and apoptosis via the endoplasmic reticulum stress pathway (Li et al., 2023). A comparable oxidative–stress–mediated mechanism may contribute to astrocyte vulnerability under PSN exposure. These findings indicate that PSNs differentially regulate glial responses, dampening astrocyte activation while promoting apoptotic cell death.

Expression of glial activation markers, including *Iba-1*, *Gfap*, and *Tgfβ1*, was significantly elevated following co-exposure to PSNs and LPS. LPS alone robustly up-regulated *Iba-1* and *Gfap*, consistent with its known ability to provoke glial reactivity and neuroinflammatory signaling within the CNS (Norden et al., 2016). *Tgfβ1*, encoding an anti-inflammatory cytokine involved in immunosuppression and tissue regeneration (Sun et al., 2018), was also significantly up-regulated upon LPS treatment, suggesting activation of regulatory mechanisms to restore homeostasis after the initial inflammatory response. In contrast, the proinflammatory cytokines *Tnfα*, *Il-6*, and *Il-10* showed nonsignificant increases (P>0.05) upon LPS treatment, indicating a tightly controlled cytokine transcriptional response during this phase of inflammation, as demonstrated previously (Qin et al., 2023). Notably, *Iba-1* expression was significantly lower in LPS-treated animals that received PSNs compared to those receiving PSNs alone. Thus, microglial dysfunction due to PSN exposure appears to induce an abnormal immune response in microglia during LPS-induced neuroinflammation.

The distinct immune responses observed in this study suggest that PSNs exert a substantial influence on neuroimmune dynamics and neuropathology. Extensive internalization of PSNs by microglia appears to drive sustained activation and elevated production of proinflammatory cytokines, in line with prior reports of microglial sensitization under chronic inflammatory stimuli (Lull & Block, 2010). Sustained activation driven by persistent PSN exposure may impair microglial regulatory functions, including synaptic pruning and homeostatic surveillance, potentially leading to synapse loss and reduced dendritic spine density—hallmarks of cognitive decline and behavioral dysfunction in murine models (Andoh & Koyama, 2021; Chen et al., 2006; Li et al., 2022; Mordelt & De Witte, 2023). These findings align with recent studies reporting behavioral abnormalities following exposure to plastic particles, underscoring their neurotoxic potential (Paing et al., 2024; So et al., 2023; Takai et al., 2022). Consistently, *in vivo* analysis revealed a significant increase in hippocampal microglia following co-exposure to PSNs and LPS, further implicating PSNs in the perturbation of CNS immune homeostasis.

This study demonstrated that PSNs accumulate within brain-resident immune cells and modulate glial responsiveness to inflammatory stimuli. Notably, PSNs suppressed LPS-induced astrocyte activation while promoting astrocyte apoptosis, revealing for the first time that PSNs may alter astrocyte viability and immune function. Furthermore, our results showed that exposure to PSNs during development may reprogram neuroimmune interactions, predisposing the CNS to aberrant inflammatory responses and increasing susceptibility to neurodegeneration. To elucidate the molecular basis of these effects, future studies should quantify ROS production, examine activation of the endoplasmic reticulum stress response, and assess expression of apoptosis-related proteins in glial populations. In addition, the influence of PSN concentration, exposure duration, and cellular context on microglial and astrocytic responses warrants systematic analysis to dissect the regulatory mechanisms governing PSN-induced neuroinflammation and its role in neurological disease progression (Marcellus et al., 2024). Furthermore, as our analysis was restricted to the cortex and hippocampus, inclusion of other brain regions,

such as the striatum and cerebellum, will be essential to identify regional vulnerabilities and define spatially distinct immunomodulatory profiles (Brandi et al., 2022). Addressing these limitations will be critical for advancing mechanistic insights into how PSNs influence neuroimmune permeability and function across diverse brain regions and contexts.

CONCLUSION

This study demonstrated that prenatal exposure to PSNs resulted in their accumulation within brain-resident immune cells, particularly microglia and astrocytes. PSN internalization enhanced microglial activation while suppressing apoptosis, indicative of prolonged neuroinflammation. In contrast, astrocytes exhibited increased apoptosis and decreased reactive morphology, suggesting divergent, cell type-specific immune dysregulation. Following long-term exposure from the fetal stage through adulthood, PSNs impaired immune responses in both microglia and astrocytes upon LPS challenge *in vivo*. Transcriptional analyses revealed abnormal activation signatures under combined PSN and LPS exposure, further supporting differential glial responses. These findings suggest that PSNs disrupt glial immune regulation through distinct mechanisms and may contribute to persistent neuroimmune dysregulation. In light of growing environmental microplastic exposure, these results highlight the potential neurotoxic risk posed by PSNs.

SUPPLEMENTARY DATA

Supplementary data to this article can be found online.

COMPETING INTERESTS

The authors declare that they have no competing interests.

AUTHORS' CONTRIBUTIONS

Y.H.S.: Writing–original draft, Investigation, Methodology, Formal analysis. H.S.S.: Methodology, Investigation. D.H.L.: Methodology, Investigation. M.J.K.: Writing–review & editing. J.Y.K.: Writing–review & editing. B.H.Y.: Writing–review & editing, E.H.L.: Writing–review & editing. E.M.J.: Writing–review & editing, Conceptualization, Methodology, Resources, Supervision, Funding acquisition. All authors read and approved the final version of the manuscript.

REFERENCES

Adamiak K, Sidoryk-Węgrzynowicz M, Dąbrowska-Bouta B, et al. 2025. Primary astrocytes as a cellular depot of polystyrene nanoparticles. *Scientific Reports*, **15**(1): 6502.

Amato-Lourenço LF, Dantas KC, Júnior GR, et al. 2024. Microplastics in the olfactory bulb of the human brain. *JAMA Network Open*, **7**(9): e2440018.

Andoh M, Koyama R. 2021. Microglia regulate synaptic development and plasticity. *Developmental Neurobiology*, **81**(5): 568–590.

Asimakidou E, Tan JKS, Zeng JL, et al. 2024. Blood-brain barrier-targeting nanoparticles: biomaterial properties and biomedical applications in translational neuroscience. *Pharmaceuticals*, **17**(5): 612.

Bani-Yaghoub M, Tremblay RG, Lei JX, et al. 2006. Role of Sox2 in the development of the mouse neocortex. *Developmental Biology*, **295**(1): 52–66.

Brandi E, Torres-Garcia L, Svanbergsson A, et al. 2022. Brain region-specific microglial and astrocytic activation in response to systemic lipopolysaccharides exposure. *Frontiers in Aging Neuroscience*, **14**: 910988.

Butovsky O, Weiner HL. 2018. Microglial signatures and their role in health and disease. *Nature Reviews Neuroscience*, **19**(10): 622–635.

Cabezas R, Ávila M, Gonzalez J, et al. 2014. Astrocytic modulation of blood brain barrier: perspectives on Parkinson's disease. *Frontiers in Cellular Neuroscience*, **8**: 211.

Casoni F, Croci L, Marroni F, et al. 2024. A spatial-temporal map of glutamatergic neurogenesis in the murine embryonic cerebellar nuclei uncovers a high degree of cellular heterogeneity. *Journal of Anatomy*, **245**(4): 560–571.

Chaiwut R, Kasinrerk W. 2022. Very low concentration of lipopolysaccharide can induce the production of various cytokines and chemokines in human primary monocytes. *BMC Research Notes*, **15**(1): 42.

Chen KQ, Iribarren P, Hu JY, et al. 2006. Activation of Toll-like receptor 2 on microglia promotes cell uptake of Alzheimer disease-associated amyloid β peptide. *Journal of Biological Chemistry*, **281**(6): 3651–3659.

Cheng J, Zhou Y, Qiao HW, et al. 2023. Curcumin protects from LPS-induced activation of astrocytes via AMPK pathway. *NeuroReport*, **34**(15): 748–758.

Chhatbar C, Prinz M. 2021. The roles of microglia in viral encephalitis: from sensome to therapeutic targeting. *Cellular & Molecular Immunology*, **18**(2): 250–258.

Da Silva AAF, Fiadeiro MB, Bernardino LI, et al. 2024. Lipopolysaccharide-induced animal models for neuroinflammation - An overview. *Journal of Neuroimmunology*, **387**: 578273.

Domenech J, Marcos R. 2021. Pathways of human exposure to microplastics, and estimation of the total burden. *Current Opinion in Food Science*, **39**: 144–151.

Fu RY, Shen QY, Xu PF, et al. 2014. Phagocytosis of microglia in the central nervous system diseases. *Molecular Neurobiology*, **49**(3): 1422–1434.

Galloway DA, Phillips AEM, Owen DRJ, et al. 2019. Phagocytosis in the brain: homeostasis and disease. *Frontiers in Immunology*, **10**: 790.

Gao C, Jiang JW, Tan YY, et al. 2023. Microglia in neurodegenerative diseases: mechanism and potential therapeutic targets. *Signal Transduction and Targeted Therapy*, **8**(1): 359.

Geyer R, Jambeck JR, Law KL. 2017. Production, use, and fate of all plastics ever made. *Science Advances*, **3**(7): e1700782.

Ghasemi A, Zahediasl S. 2012. Normality tests for statistical analysis: a guide for non-statisticians. *International Journal of Endocrinology and Metabolism*, **10**(2): 486–489.

Goshi N, Lam D, Bogguri C, et al. 2025. Direct effects of prolonged TNF-α and IL-6 exposure on neural activity in human iPSC-derived neuron-astrocyte co-cultures. *Frontiers in Cellular Neuroscience*, **19**: 1512591.

Haanen C, Vermes I. 1995. Apoptosis and inflammation. *Mediators of Inflammation*, **4**(1): 5–15.

Haruwaka K, Ikegami A, Tachibana Y, et al. 2019. Dual microglia effects on blood brain barrier permeability induced by systemic inflammation. *Nature Communications*, **10**(1): 5816.

He YB, Taylor N, Yao X, et al. 2021. Mouse primary microglia respond differently to LPS and poly(I: C) in vitro. *Scientific Reports*, **11**(1): 10447.

Hickman S, Izzy S, Sen P, et al. 2018. Microglia in neurodegeneration. *Nature Neuroscience*, **21**(10): 1359–1369.

Huang YJ, Liang BX, Li ZM, et al. 2023. Polystyrene nanoplastic exposure induces excessive mitophagy by activating AMPK/ULK1 pathway in differentiated SH-SY5Y cells and dopaminergic neurons in vivo. *Particle and Fibre Toxicology*, **20**(1): 44.

Jenner LC, Rotchell JM, Bennett RT, et al. 2022. Detection of microplastics in human lung tissue using μFTIR spectroscopy. *Science of the Total Environment*, **831**: 154907.

Jung EM, Choi KC, Yu FH, et al. 2010. Effects of 17β-estradiol and xenoestrogens on mouse embryonic stem cells. *Toxicology in Vitro*, **24**(6): 1538–1545.

Jung EM, Moffat JJ, Liu JX, et al. 2017. *Arid1b* haploinsufficiency disrupts cortical interneuron development and mouse behavior. *Nature*

Neuroscience, **20**(12): 1694–1707.
Kaur M, Sharma A, John P, et al. 2024. Manifestation of polystyrene microplastic accumulation in brain with emphasis on morphometric and histopathological changes in limbic areas of Swiss albino mice. *Neurotoxicology*, **105**: 231–246.
Kaushik A, Singh A, Kumar Gupta V, et al. 2024. Nano/micro-plastic, an invisible threat getting into the brain. *Chemosphere*, **361**: 142380.
Kershaw PJ, Rochman CM. 2015. Sources, fate and effects of microplastics in the marine environment: part 2 of a global assessment. London: International Maritime Organization.
Kim DY, Park MK, Yang HW, et al. 2025. Effects of microplastic accumulation on neuronal death after global cerebral ischemia. *Cells*, **14**(4): 241.
Kim Y, Park J, Choi YK. 2019. The role of astrocytes in the central nervous system focused on BK channel and heme oxygenase metabolites: a review. *Antioxidants*, **8**(5): 121.
Konishi H, Koizumi S, Kiyama H. 2022. Phagocytic astrocytes: emerging from the shadows of microglia. *Glia*, **70**(6): 1009–1026.
Kopatz V, Wen K, Kovács T, et al. 2023. Micro- and nanoplastics breach the blood-brain barrier (BBB): biomolecular corona's role revealed. *Nanomaterials*, **13**(8): 1404.
Kwon W, Kim D, Kim HY, et al. 2022. Microglial phagocytosis of polystyrene microplastics results in immune alteration and apoptosis *in vitro* and *in vivo*. *Science of the Total Environment*, **807**: 150817.
Lee SH, Shin HS, So YH, et al. 2024. Maternal exposure to 4-tert-octylphenol causes alterations in the morphology and function of microglia in the offspring mouse brain. *Journal of Hazardous Materials*, **480**: 136258.
Leslie HA, van Velzen MJM, Brandsma SH, et al. 2022. Discovery and quantification of plastic particle pollution in human blood. *Environment International*, **163**: 107199.
Li N, Deng MR, Hu GH, et al. 2022. New insights into microglial mechanisms of memory impairment in Alzheimer's disease. *Biomolecules*, **12**(11): 1722.
Li Z, Xu T, Peng L, et al. 2023. Polystyrene nanoplastics aggravates lipopolysaccharide-induced apoptosis in mouse kidney cells by regulating IRE1/XBP1 endoplasmic reticulum stress pathway via oxidative stress. *Journal of Cellular Physiology*, **238**(1): 151–164.
Liu B, Wang K, Gao HM, et al. 2001. Molecular consequences of activated microglia in the brain: overactivation induces apoptosis. *Journal of neurochemistry*, **77**(1): 182–189.
Liu J, Kang R, Tang DL. 2024. Lipopolysaccharide delivery systems in innate immunity. *Trends in Immunology*, **45**(4): 274–287.
Liu X, Ying J, Wang XF, et al. 2021. Astrocytes in neural circuits: key factors in synaptic regulation and potential targets for neurodevelopmental disorders. *Frontiers in Molecular Neuroscience*, **14**: 729273.
Lively S, Schlichter LC. 2018. Microglia responses to pro-inflammatory stimuli (LPS, IFNγ+TNFα) and reprogramming by resolving cytokines (IL-4, IL-10). *Frontiers in Cellular Neuroscience*, **12**: 215.
Liverani E, Rico MC, Yaratha L, et al. 2014. LPS-induced systemic inflammation is more severe in $P2Y_{12}$ null mice. *Journal of Leukocyte Biology*, **95**(2): 313–323.
Lull ME, Block ML. 2010. Microglial activation and chronic neurodegeneration. *Neurotherapeutics*, **7**(4): 354–365.
Luo RQ, Yao YX, Chen Z, et al. 2025. An examination of the LPS-TLR4 immune response through the analysis of molecular structures and protein–protein interactions. *Cell Communication and Signaling*, **23**(1): 142.
Marcellus KA, Bugiel S, Nunnikhoven A, et al. 2024. Polystyrene nano- and microplastic particles induce an inflammatory gene expression profile in rat neural stem cell-derived astrocytes in vitro. *Nanomaterials*, **14**(5): 429.
Mordelt A, De Witte LD. 2023. Microglia-mediated synaptic pruning as a key deficit in neurodevelopmental disorders: hype or hope?. *Current Opinion in Neurobiology*, **79**: 102674.
Nihart AJ, Garcia MA, El Hayek E, et al. 2025. Bioaccumulation of microplastics in decedent human brains. *Nature Medicine*, **31**(4): 1114–1119.
Norden DM, Trojanowski PJ, Villanueva E, et al. 2016. Sequential activation of microglia and astrocyte cytokine expression precedes increased Iba-1 or GFAP immunoreactivity following systemic immune challenge. *Glia*, **64**(2): 300–316.
Özsoy S, Gündogdu S, Sezigen S, et al. 2024. Presence of microplastics in human stomachs. *Forensic Science International*, **364**: 112246.
Paing YMM, Eom Y, Song GB, et al. 2024. Neurotoxic effects of polystyrene nanoplastics on memory and microglial activation: insights from *in vivo* and *in vitro* studies. *Science of the Total Environment*, **924**: 171681.
Panchenko PE, Hippauf L, Konsman JP, et al. 2023. Do astrocytes act as immune cells after pediatric TBI?. *Neurobiology of Disease*, **185**: 106231.
Pascual O, Ben Achour S, Rostaing P, et al. 2012. Microglia activation triggers astrocyte-mediated modulation of excitatory neurotransmission. *Proceedings of the National Academy of Sciences of the United States of America*, **109**(4): E197–E205.
Pham DT, Kim J, Lee SH, et al. 2023. Analysis of microplastics in various foods and assessment of aggregate human exposure via food consumption in korea. *Environmental Pollution*, **322**: 121153.
Qin J, Ma ZH, Chen XL, et al. 2023. Microglia activation in central nervous system disorders: a review of recent mechanistic investigations and development efforts. *Frontiers in Neurology*, **14**: 1103416.
Ragusa A, Svelato A, Santacroce C, et al. 2021. Plasticenta: first evidence of microplastics in human placenta. *Environment International*, **146**: 106274.
Ransohoff RM, Brown MA. 2012. Innate immunity in the central nervous system. *The Journal of Clinical Investigation*, **122**(4): 1164–1171.
Senathirajah K, Attwood S, Bhagwat G, et al. 2021. Estimation of the mass of microplastics ingested–a pivotal first step towards human health risk assessment. *Journal of Hazardous Materials*, **404**: 124004.
Shapiro SS, Wilk MB. 1965. An analysis of variance test for normality (complete samples). *Biometrika*, **52**(3-4): 591–611.
Shin HS, Lee SH, Moon HJ, et al. 2023. Exposure to polystyrene particles causes anxiety-, depression-like behavior and abnormal social behavior in mice. *Journal of Hazardous Materials*, **454**: 131465.
So YH, Shin HS, Lee SH, et al. 2023. Maternal exposure to polystyrene microplastics impairs social behavior in mouse offspring with a potential neurotoxicity. *Neurotoxicology*, **99**: 206–216.
Sun L, Xiu M, Wang SH, et al. 2018. Lipopolysaccharide enhances TGF-β1 signalling pathway and rat pancreatic fibrosis. *Journal of Cellular and Molecular Medicine*, **22**(4): 2346–2356.
Takai Y, Tokusumi H, Sato M, et al. 2022. Combined effect of diazepam and polystyrene microplastics on the social behavior of medaka (*Oryzias latipes*). *Chemosphere*, **299**: 134403.
Tanaka T, Narazaki M, Kishimoto T. 2014. IL-6 in inflammation, immunity, and disease. *Cold Spring Harbor Perspectives in Biology*, **6**(10): a016295.
Thion MS, Garel S. 2017. On place and time: microglia in embryonic and perinatal brain development. *Current Opinion in Neurobiology*, **47**: 121–130.
Tohidpour A, Morgun AV, Boitsova EB, et al. 2017. Neuroinflammation and infection: molecular mechanisms associated with dysfunction of neurovascular unit. *Frontiers in Cellular and Infection Microbiology*, **7**: 276.
Tran M, Heo C, Lee LP, et al. 2022. Human mini-blood-brain barrier models for biomedical neuroscience research: a review. *Biomaterials Research*, **26**(1): 82.
Vidal-Itriago A, Radford RAW, Aramideh JA, et al. 2022. Microglia morphophysiological diversity and its implications for the CNS. *Frontiers in Immunology*, **13**: 997786.
Wicks EE, Ran KR, Kim JE, et al. 2022. The translational potential of

microglia and monocyte-derived macrophages in ischemic stroke. *Frontiers in Immunology*, **13**: 897022.

Wilhelmsson U, Bushong EA, Price DL, et al. 2006. Redefining the concept of reactive astrocytes as cells that remain within their unique domains upon reaction to injury. *Proceedings of the National Academy of Sciences of the United States of America*, **103**(46): 17513–17518.

Xu P, Shan C, Dunn TJ, et al. 2020. Role of microglia in the dissemination of Zika virus from mother to fetal brain. *PLoS Neglected Tropical Diseases*, **14**(7): e0008413.

Xu P, Yu YJ, Wu P. 2024. Role of microglia in brain development after viral infection. *Frontiers in Cell and Developmental Biology*, **12**: 1340308.

Zhao YX, Huang YY, Cao Y, et al. 2024. Astrocyte-mediated neuroinflammation in neurological conditions. *Biomolecules*, **14**(10): 1204.

Zhou B, Zuo YX, Jiang RT. 2019. Astrocyte morphology: diversity, plasticity, and role in neurological diseases. *CNS Neuroscience & Therapeutics*, **25**(6): 665–673.

Ziebell JM, Adelson PD, Lifshitz J. 2015. Microglia: dismantling and rebuilding circuits after acute neurological injury. *Metabolic Brain Disease*, **30**(2): 393–400.